Cell Reports, Volume *30*

Supplemental Information

Vesicle Shrinking and Enlargement Play Opposing Roles in the Release of Exocytotic Contents

Wonchul Shin, Gianvito Arpino, Sathish Thiyagarajan, Rui Su, Lihao Ge, Zachary McDargh, Xiaoli Guo, Lisi Wei, Oleg Shupliakov, Albert Jin, Ben O'Shaughnessy, and Ling-Gang Wu

Supplementary Figures

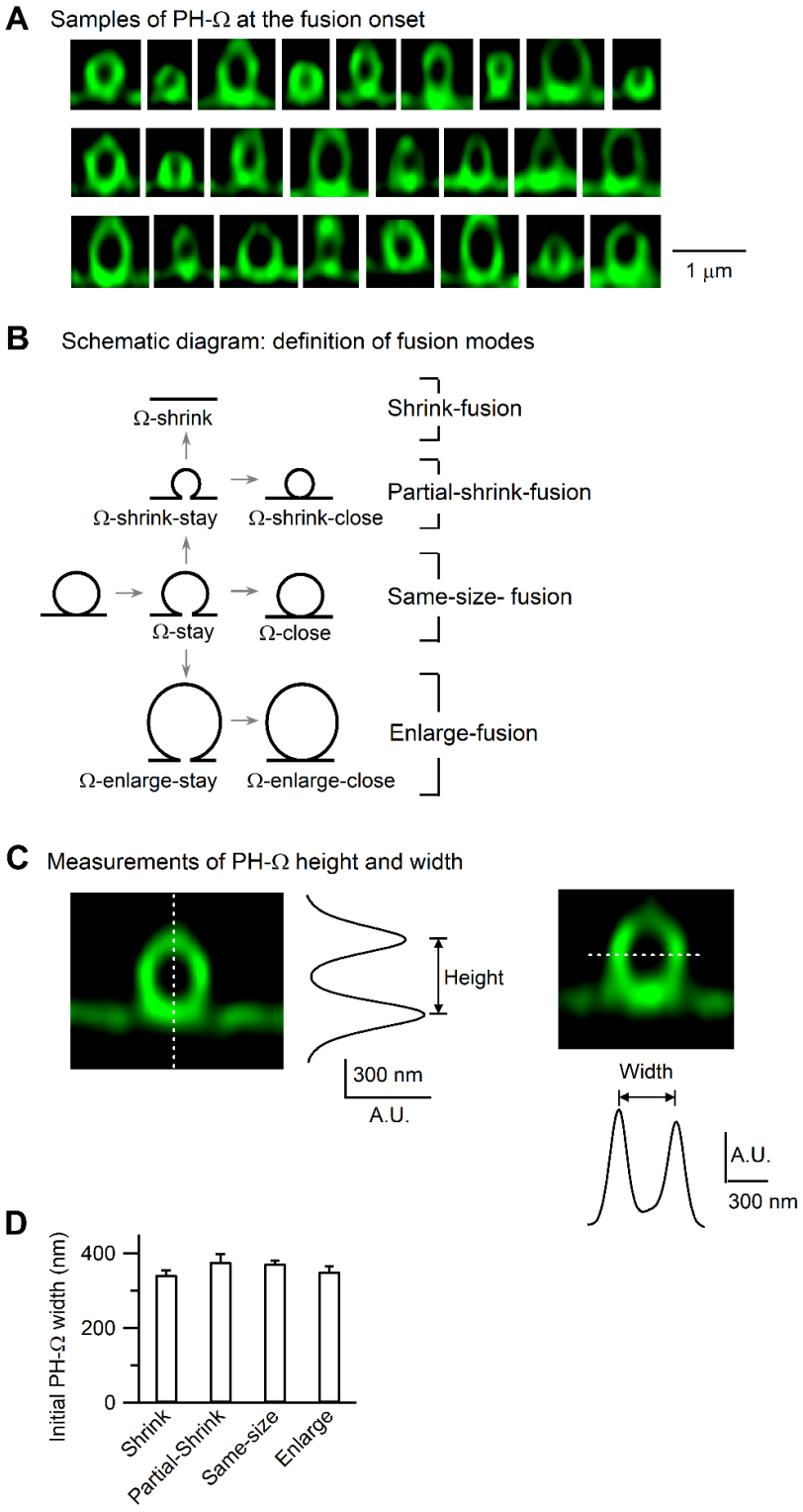

Figure S1. Measurements of PH-Ω size, Related to Figure 1.

(A) Additional samples of PH-Ω observed at the fusion onset. Each PH-Ω was from a different cell during xz/y_{fix} STED scanning.

(B) A schematic diagram showing size-related fusion modes suggested based on imaging of soluble dyes labelling the fusing Ω-profile's lumen: 1) shrink-fusion, 2) partial-shrink-fusion, 3) same-size-fusion, and 4) enlarge-fusion. Except shrink-fusion, every category includes two modes, one with pore remained open, the other with pore closure sometime after fusion. Thus, partial-shrink fusion includes Ω-shrink-stay (pore remained open) and Ω-shrink-close (pore closure after fusion); same-size-fusion includes Ω-stay (pore remained open) and Ω-close (pore closure after fusion); enlarge-fusion includes enlarge-stay (pore remained open) and Ω-enlarge-close (pore remained open).

(C) Measurement of the PH-Ω's height and width during STED xz/y_{fix} imaging.
Left: a PH_G-labelled Ω-profile, and the PH_G fluorescence profile across the dotted line. The distance between the two peaks of the PH_G line profile is taken as the height of the PH-Ω.
Right: a PH_G-labelled Ω-profile (upper) and the PH_G fluorescence profile across the dotted line (lower). The distance between the two peaks of the PH_G line profile is taken as the width of the PH-Ω.

(D) Similar PH-Ω width observed for shrink-fusion, partial-shrink-fusion, same-size-fusion and enlarge-fusion (total fusion event number: 236; from 202 cells). No statistical differences were found ($p > 0.05$, ANOVA test).

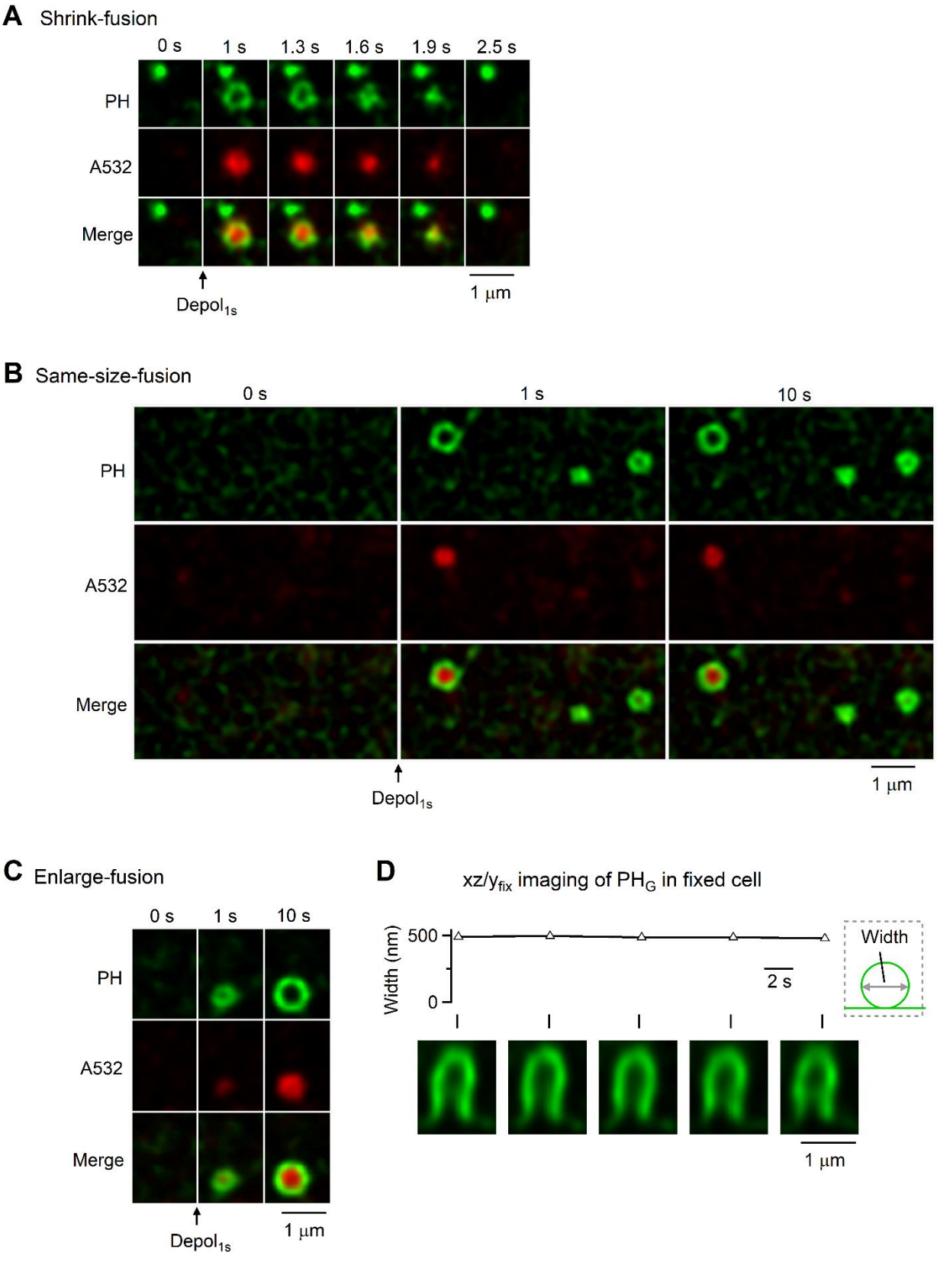
A Shrink-fusion
0 s
1 s
1.3 s
1.6 s
1.9 s
2.5 s
PH
A532
Merge
Depol1s
1 μm
B Same-size-fusion
0 s
1 s
10 s
PH
A532
Merge
Depol1s
1 μm
C Enlarge-fusion
0 s
1 s
10 s
PH
A532
Merge
Depol1s
1 μm
D
xz/yfix imaging of PHG in fixed cell
Width (nm)
500
0
2 s
Width
1 μm

Figure S2. Ω-profiles do not move at the xy plane, Related to Figure 1.

(A-C) STED xy/z_{fix} imaging of PH_G (upper, green) and A532 (red, in the bath, middle) in live chromaffin cells shows three $depol_{1s}$-induced PH_G rings with A532 spots (lower, green and red channels merged), the size of which may A) shrink (shrink-fusion), B) remain unchanged (same-size-fusion), or C) enlarge (enlarge-fusion) at various times as labelled after $depol_{1s}$. In all three conditions, PH_G-labelled rings or A532 spots did not move at the xy-plane. For shrink-fusion in panel A, a pre-existing PH_G spot before $depol_{1s}$ serves as the marker showing the stability of our imaging system. For same-size-fusion in panel B, three same-size-fusion events did not change their relative position at the xy-plane.

(D) STED xz/y_{fix} imaging of PH_G in a 4%-paraformaldehyde-fixed chromaffin cell shows a PH-Ω that did not change in width throughout the 24 s imaging time.

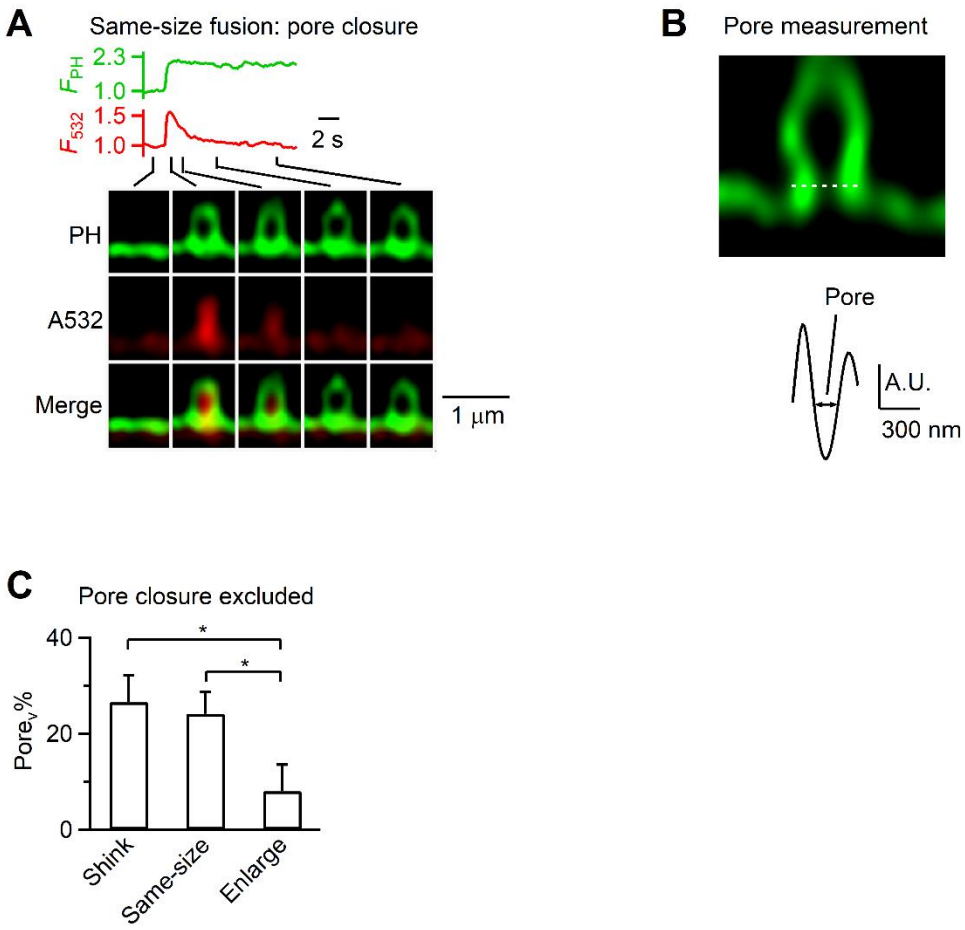

Figure S3. Pore measurements during STED xz/y_{fix} imaging of PH_G/A532, Related to Figure 3.

(A) PH-Ω fluorescence (F_{PH}, normalized to baseline), A532 spot fluorescence (F_{532}, normalized to baseline), of sampled images at times indicated with lines showing a vesicle undergoing Ω-stay fusion. F_{532} (strong excitation) decay to the baseline while F_{PH} was stable reflected pore closure that prevented the bleached A532 (caused by strong excitation) from exchange with fluorescent A532 in the bath. Images were acquired at the STED xz/y_{fix} configuration.

(B) Measurement of the PH-Ω's pore width during STED xz/y_{fix} imaging. A PH_G-labelled Ω-profile (upper) and the PH_G fluorescence profile across the dotted line (lower). The half width of the V-shape valley of the fluorescence profile is taken as the pore width, which, has been shown by simulation to reflect the pore diameter (see Shin et al., 2018 for detail).

(C) The percentage of observing a $Pore_v$ during $shrink_{related}$-fusion, same-size-fusion and enlarge-fusion. The data were taken from Figure 3I (total fusion event number: 236; from 202 cells), except that the fusion pore closure events were not included. *: $p < 0.05$, ANOVA test.

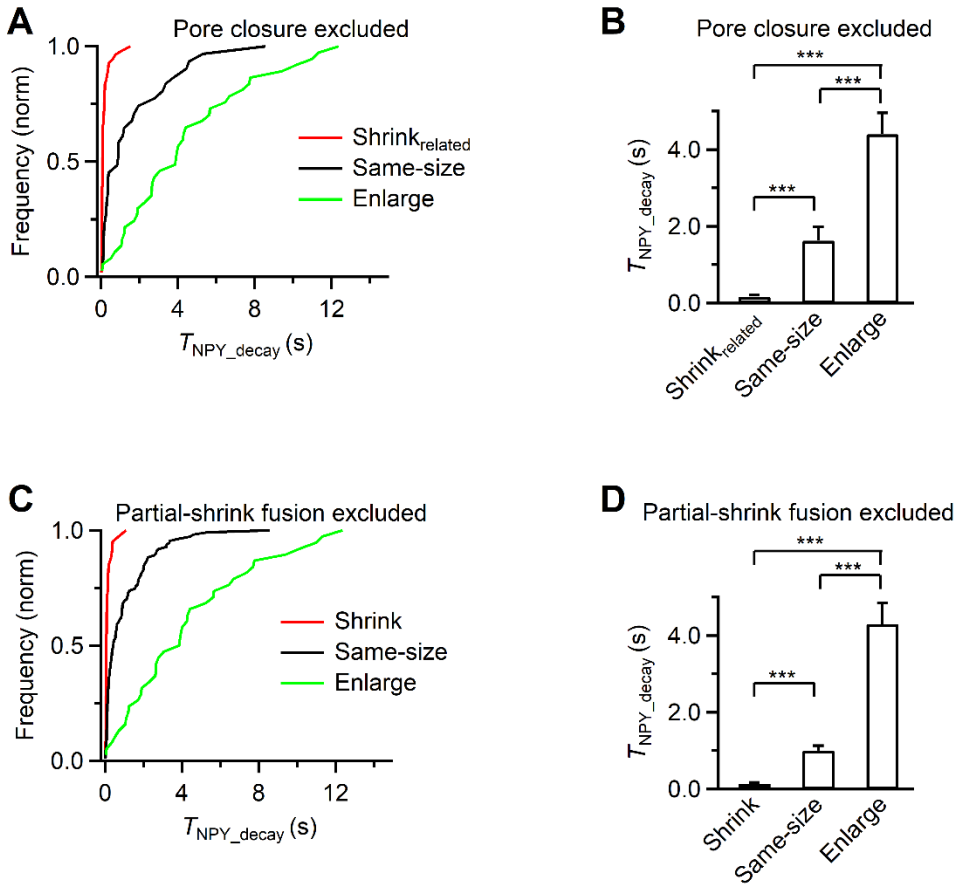

Figure S4. Shrink$_{related}$-fusion speeds up NPY-EGFP release and enlarge-fusion slows down NPY-EGFP release, Related to Figure 4.

(A-B) Cumulative frequency (A, normalized) or the 20-80% F_{NPY} decay time (T_{NPY_decay}, B) for shrink$_{related}$-fusion (55 events, 28 cells), size-similar-fusion (31 events, 28 cells) and enlarge-fusion (37 events, 28 cells). Panels A-B are the same as Figure 4H-I, except that the pore closure events (Ω-shrink-close, Ω-close, Ω-enlarge-close) are not included for analysis. T_{NPY_decay} is expressed as mean + s.e.m. The results in panels A-B are analogous to those shown in Figure 4H-I.

(C-D) Cumulative frequency (C, normalized) or T_{NPY_decay} (D, mean + s.e.m.) for shrink-fusion (41 events, 28 cells), size-similar-fusion (111 events, 28 cells) and enlarge-fusion (38 events, 28 cells). These plots are similar to Figure 4H-I, except that shrink$_{related}$-fusion (including Ω-shrink, Ω-shrink-stay and Ω-shrink-close) is replaced with shrink-fusion.

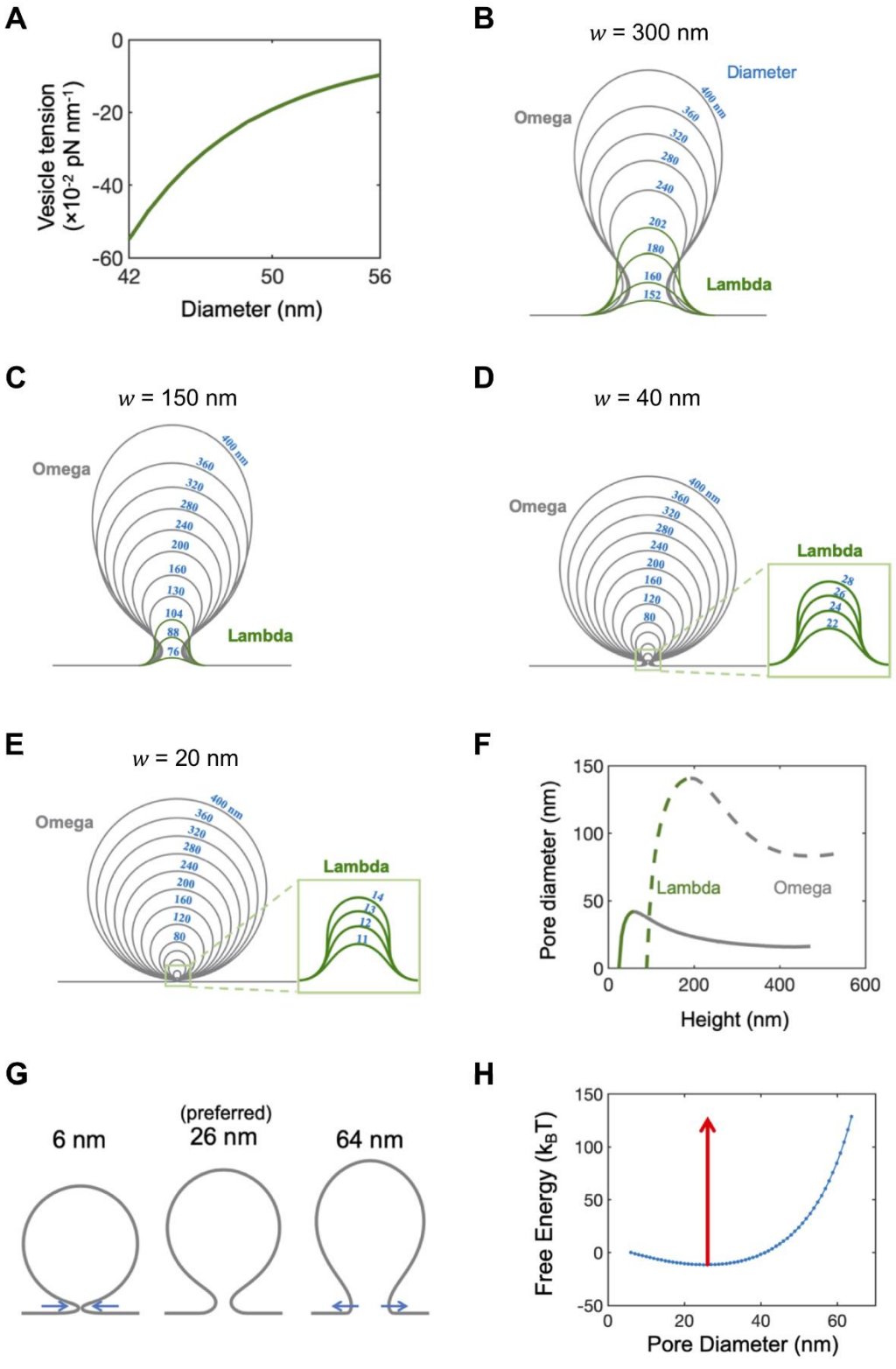
A
0
-20
-40
-60
Vesicle tension
(×10-2 pN nm-1)
42
50
56
Diameter (nm)
B
w = 300 nm
Diameter
Omega
400 nm
360
320
280
240
202
180
160
152
Lambda
C
w = 150 nm
Omega
400 nm
360
320
280
240
200
160
130
104
88
76
Lambda
D
w = 40 nm
Omega
400 nm
360
320
280
240
200
160
120
80
Lambda
28
26
24
22
E
w = 20 nm
Omega
400 nm
360
320
280
240
200
160
120
80
Lambda
14
13
12
11
F
150
100
50
0
Pore diameter (nm)
Lambda
Omega
0
200
400
600
Height (nm)
G
6 nm
(preferred)
26 nm
64 nm
H
150
100
50
0
-50
Free Energy (kBT)
0
20
40
60
Pore Diameter (nm)

Figure S5. Modelling of Ω-profile shrinking, Related to Figure 5.

(A) Vesicle membrane tension versus effective diameter D (vesicle area equals πD^2) for Λ-shape of Fig. 5B.

(B-E) The predicted sequences of shapes are calculated for diameter of actin cortex-free zone w equal to (B) 300 nm, (C) 150 nm. (D) 40 nm and (E) 20 nm, respectively. The four sequences show that the Ω-to-Λ transitions in the shrink trajectory occur at effective diameter D of (B) 202 nm, (C) 104 nm, (D) 28 nm and (E) 14 nm, respectively. Conclusion: a large w leads to earlier Ω-to-Λ transition while for small w values, Λ shapes are adopted at smaller sizes.

(F) Vesicle pore diameter versus vesicle height with diameter of actin cortex-free zone w equal to 80 nm (solid line) or 300 nm (dashed line). The largest vesicle in each sequence has an effective diameter of 400 nm. For Λ shapes, the pore diameter is defined to be the vesicle width at fixed height. This height is chosen to be the height of the fusion pore of the last Ω-shaped vesicle before the transition to the Λ regime.

(G) Three examples of minimum energy shapes of fused vesicles calculated with Monte Carlo method. The constrained pore diameter for each shape is shown in the label above. The vesicle diameter is 200 nm. The energetically preferred pore diameter is ~26 nm as at that diameter no external force is needed to constrain the pore size.

(H) Free energy landscape of fusion pore expansion. An energy barrier of ~140 k_BT (red arrow) is needed to expand the fusion pore from the preferred size to 80% of the diameter of the actin cortex-free zone.